Inorganic Chemistry

Article

pubs.acs.org/IC

Further Evidence for the Stabilization of U(V) within a Tetraoxo Core

Jared T. Stritzinger,[†] Evgeny V. Alekseev,*[,‡] Matthew J. Polinski,[†] Justin N. Cross,[†] Teresa M. Eaton,[†] and Thomas E. Albrecht-Schmitt*[,†]

[†]Department of Chemistry and Biochemistry, Florida State University, 95 Chieftan Way, Tallahassee, Florida 32306-4390, United States

[‡]Institute for Energy and Climate Research (IEK-6), Forschungszentrum Jülich GmbH, Germany and Institut für Kristallographie, RWTH Aachen University, 52428 Jülich, 52066 Aachen, Germany

Supporting Information

ABSTRACT: Two complex layered uranyl borates, $K_{10}[(UO_2)_{16}(B_2O_5)_2(BO_3)_6O_8]\cdot 7H_2O$ (**1**) and $K_{13}[(UO_2)_{19}(UO_4)(B_2O_5)_2(BO_3)_6(OH)_2O_5]\cdot H_2O$ (**2**), were isolated from supercritical water reactions. Within these compounds, borate exists only as BO_3 units and is found as either isolated BO_3 triangles or B_2O_5 dimers, the latter being formed from corner sharing of two BO_3 units. These anions, along with oxide and hydroxide, bridge between uranyl centers to create the complex layers in these compounds. U(VI) cations are found within uranyl, UO_2^{2+} units, that are bound by four or five oxygen atoms to create tetragonal and pentagonal bipyramidal environments. The most striking feature in this system is found in **2**, where a $[UO_4(OH)_2]$ unit exists that contains U(V) within a tetraoxo core with trans hydroxide anions; therefore, this compound is a mixed-valent U(VI)/U(V) borate. The presence of a $5f^1$ uranium site within **2** leads to unusual optical properties.

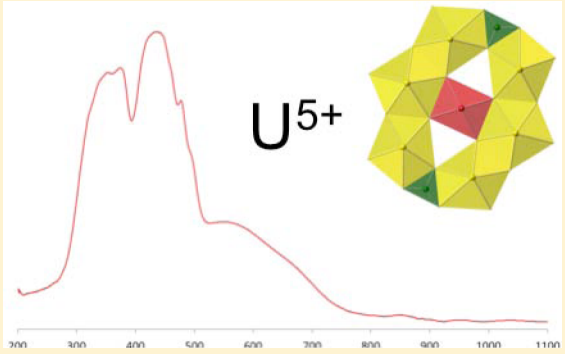

INTRODUCTION

Variable oxidation states are a prevalent feature of the early actinides, and uranium is an excellent example of this, existing in all oxidation states between 2+ and 6+.[1,2] However, in the presence of air and water, only the IV and VI oxidation states are common.[1] The preparation of U(V) compounds is often problematic in aqueous media because U(V) rapidly disproportionates into U(VI) and U(IV).[3,4] Despite this, U(V) compounds are becoming better represented in the literature owing to new and nontraditional synthetic methodologies that are able to circumvent disproportionation pathways.[5,6] Among the most promising of the new techniques employed for preparing uncommon valence states for uranium is the use of supercritical water as a reaction medium. Lii and co-workers have championed this method and provided numerous examples of mixed-valent uranium silicates and germanates, one of which simultaneously contains U(IV), U(V), and U(VI).[7]

Uranium's variable coordination chemistry leads to vast structural diversity. In low oxidation states, high coordination numbers of eight and nine are common, and the coordination is relatively isotropic. When the oxidation state is raised to V or VI, trans terminal oxo groups are typically present, and this leads to highly anisotropic coordination and environments that take the form of bipyramids with four to six donor atoms in the equatorial plane perpendicular to an AnO_2^{n+} core. Although the most common U(VI) structural unit is the UO_7 pentagonal bipyramid, there are compounds that contain uranium in as many as three different coordination environments simultaneously.[8,9]

Our group has been interested in the preparation of novel actinide borates from thorium to californium in oxidation states from III to VI.[10,11] Neptunium borates show remarkably rich redox chemistry and mixed valency is common.[12] However, all uranium borates to date contain only U(VI). The use of supercritical water as a reaction medium can provide a route to lower oxidation states of uranium to link uranium and neptunium borate chemistry. Herein we disclose the preparation, crystal structures, and optical properties of two new uranium borates obtained from supercritical water reactions. One of these compounds is the first example of a mixed-valent U(VI)/U(V) borate, thereby bridging uranium and neptunium borate chemistry.

EXPERIMENTAL SECTION

Syntheses. UO_3 (Bioanalytical Industries, 99.5%), $KBO_2\cdot xH_2O$ (Alfa Aesar, 99.5% min), B_2O_3 (Alfa Aesar, 99.5% min), and KOH (Alfa Aesar) were used as received. Both uranyl borates were synthesized from reactions carried out in silver ampules (6.35 cm × 0.635 cm i.d.). Reactants and mineralizer were loaded into the ampules and welded shut. The ampules were loaded into a 27 mL internal volume autoclave, utilizing a Tuttle "'cold seal'" plunger, and were counter-pressured with 20.0 mL of deionized water. The autoclave was heated to 600 °C and generated approximately 200 MPa for 4 days.

Received: March 6, 2014
Published: May 1, 2014

 © 2014 American Chemical Society dx.doi.org/10.1021/ic500523a | *Inorg. Chem.* 2014, 53, 5294−5299

The autoclave was removed and cooled under house air for 2 h. The ampules were removed and opened. Products were flushed out with deionized water. The yield for various phases could not be accurately calculated because residual products and amorphous material adhere to the walls of the ampule and are compressed into inaccessible pockets due to the high pressure.

Caution! *UO_3 used in this study contained depleted uranium; standard precautions for handling radioactive materials should be followed.*

Syntheses of $K_{10}[(UO_2)_{16}(B_2O_5)_2(BO_3)_6O_8]\cdot 7H_2O$ (1). A total of 178 mg of UO_3 (47.1 mg, 0.16 mmol) and $KBO_2\cdot xH_2O$ (131.1 mg, 1.60 mmol) (molar ratio 1:10) was loaded into a silver ampule. KOH (0.4 mL, 1 M) was added before the ampule was sealed. Yellow rod-shaped crystals were isolated for further study in an estimated 50% yield.

Syntheses of $K_{13}[(UO_2)_{19}(UO_4)(B_2O_5)_2(BO_3)_6(OH)_2O_5]\cdot H_2O$ (2). A total of 220 mg of UO_3 (68.4 mg, 0.25 mmol) and B_2O_3 (177.0 mg, 2.5 mmol) (molar ratio 1:10) was loaded into a silver ampule. KOH (0.4 mL, 1 M) was added before the ampule was sealed. Dichroic black/amber tablet-shaped crystals were isolated in an estimated 25% yield.

Crystallographic Studies. Crystals suitable for X-ray diffraction were isolated and mounted on CryoLoops with Krytox oil and optically aligned on a Bruker APEXII Quazar X-ray diffractometer using a digital camera. Initial intensity measurements were performed using an IμS X-ray source, a 30 W microfocused sealed tube (Mo Kα, λ = 0.71073 Å) with high-brilliance, and high-performance focusing multilayer optics. Standard APEXII software was used for determination of the unit cells and data collection control. The intensities of reflections of a sphere were collected by a combination of four sets of exposures (frames). Each set had a different φ angle for the crystal, and each exposure covered a range of 0.5° in ω. A total of 1464 frames were collected with an exposure time per frame of 10−30 s, depending on the crystal. SAINT software was used for data integration, including Lorentz and polarization corrections. Absorption corrections were applied using the program SCALE (SADABS). Relevant crystallographic information is listed in Table 1.

Table 1. Crystallographic Data for $K_{10}[(UO_2)_{16}(B_2O_5)_2(BO_3)_6O_8]\cdot 7H_2O$ (1) and $K_{13}[(UO_2)_{19}(UO_4)(B_2O_5)_2(BO_3)_6(OH)_2O_5]\cdot H_2O$ (2)

compound	1	2
mass	5555.58	13 409.8
color and habit	yellow, tablet	amber, tablet
space group	$Pmc2_1$	$Pbam$
a (Å)	11.9312(3)	13.3979(8)
b (Å)	6.8866(2)	49.867(3)
c (Å)	23.5320(6)	6.9305(4)
V (Å^3)	1933.52(9)	4630.3(5)
Z	2	2
T (K)	100	100
λ (Å)	0.71073	0.71073
maximum 2θ (deg)	27.50	27.31
ρ_{calcd} (g cm^{-3})	4.771	4.809
μ (Mo Kα) (cm^{-1})	340.26	355.22
$R(F)$ for $F_0{}^2 > 2\sigma(F_0{}^2)^a$	0.0238	0.0393
$R_w(F_0{}^2)^b$	0.0563	0.099

$^aR(F) = \sum||F_0| - |F_c||/\sum|F_0|$. $^bR(F_0^2) = [\sum w(F_0^2 - F_c^2)^2/\sum w(F_0^4)]^{1/2}$.

UV−Vis−NIR Spectroscopy. UV−vis−NIR spectra were acquired from single crystals using a Craic Technologies microspectrophotometer. Crystals were isolated in Krytox oil and placed on quartz slides. Spectra were collected from 200 to 1100 nm. The exposure times were auto-optimized by the Craic software.

Raman Spectroscopy. Raman spectra were acquired from single crystals using a Craic Technologies Apollo microspectrophotometer with laser emission at 785 nm. Data were acquired from 100 to 2100 cm^{-1} with 5 s exposures. Raman spectra can be found in the Supporting Information.

Scanning Electron Microscopy and Energy-Dispersive X-ray Spectrometry (SEM−EDS) Analysis. SEM−EDS images and data were collected using a JEOL 5900 with an XRF energy-dispersive X-ray spectrometer. The energy of the electron beam was set at 29.02 kV, and the spectrum acquisition time was 60 s. Spectra and analysis can be found in the Supporting Information.

RESULTS AND DISCUSSION

Synthesis. Water becomes a supercritical fluid at 374 °C and 22.4 MPa.[13] It is a unique medium for crystal growth because the decrease of the dielectric constant at supercritical temperatures causes reduced solubility of ions.[14] The supercritical nature of the fluid also leads to rapid mixing of the components. The conditions for hydrothermal reactions in metal vessels are known to favor reducing environments. However, this is poorly understood, and there has been considerable speculation on the nature of the reducing agent.[15] One possibility is the permeation of H_2 through the metal ampules from the outside environment.[16] Additionally, the vessel's metal wall may become involved in the reaction, resulting in another pathway for the reduction and stabilization of lower-valent metals.[17] The pH of the system is kept basic to prevent oxidation of the silver ampule, which provides OH^- anions that act as a mineralizer.[18] The combination of temperature, pressure, and pH drastically shifts the Eh of the system, potentially stabilizing unusual species in solution.[16] Furthermore, high temperatures favor BO_3 over BO_4, leading to simpler borate building units.

Structure and Topological Descriptions. $K_{10}[(UO_2)_{16}(B_2O_5)_2(BO_3)_6O_8]\cdot 7H_2O$ (1). $K_{10}[(UO_2)_{16}(B_2O_5)_2(BO_3)_6O_8]\cdot 7H_2O$ (**1**) is a layered structure that crystallizes in the polar, orthorhombic space group $Pmc2_1$. The layers are composed of a complex sheet of uranium and boron that propagate parallel to the [bc] plane, with the inner layer occupied by K^+ cations and water molecules (Figure 1). There are eight crystallographically unique uranium sites that lead to the large [bc] plane dimensions of 11.9312(3) × 23.5320(6) Å. Seven of the uranium centers are surrounded by seven oxygen atoms, creating UO_7 pentagonal bipyramidal environments that are fairly distorted in their geometries. The final uranium site is a six-coordinate tetragonal bipyramid.

The uranyl U≡O bond distances range from 1.79(1) to 1.807(8) Å for the seven-coordinate pentagonal bipyramids and 1.793(8) Å (×2) in the tetragonal bipyramid. The equatorial interactions range from 2.16(1) to 2.60(1) Å and 2.22(1) to 2.34(1) Å in the pentagonal and tetragonal bipyramids, respectively.

The sheet topology in **1** is quite complex. An anion topology representation of the layers is shown in Figure 1b. It is possible to separate two slightly different fragments (A and B, as shown in Figure 1b). Each of these fragments is based on corrugated infinite chains (shown in dark gray in Figure 1b). These chains are composed of edge-sharing UO_7 pentagonal bipyramids and can be designated as P-chains (pentagonal).[18] The structure of these chains is very similar, but in the B fragment, these chains are rotated by 180° compared with the chain orientation in the A fragment. The chains from different fragments are linked through BO_3 triangles (shown in green) and additional UO_6 and UO_7 polyhedra (shown in violet). There are only UO_7 polyhedra within the A fragment and only UO_6 within the B fragments. These additional polyhedra are linked to other U-chains via edge sharing within the fragments and via corner

dx.doi.org/10.1021/ic500523a | Inorg. Chem. 2014, 53, 5294−5299

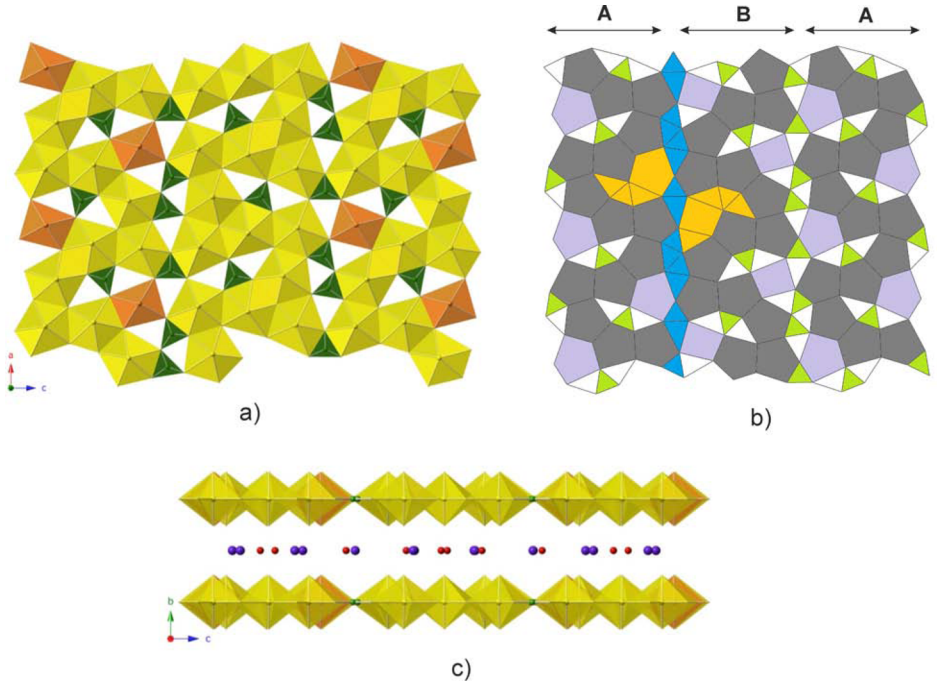

Figure 1. (a) View along the *b* axis of a portion of the structure of $K_{10}[(UO_2)_{16}(B_2O_5)_2(BO_3)_6O_8]\cdot 7H_2O$ (**1**) depicting all of the different coordination environments. (b) Anionic topology representation of the layer. (c) View of the interlayer containing K^+ cations and water. Uranium is represented by yellow and orange polyhedra, borate is represented by green triangles, oxygen is represented by red spheres, and K^+ is represented by blue spheres.

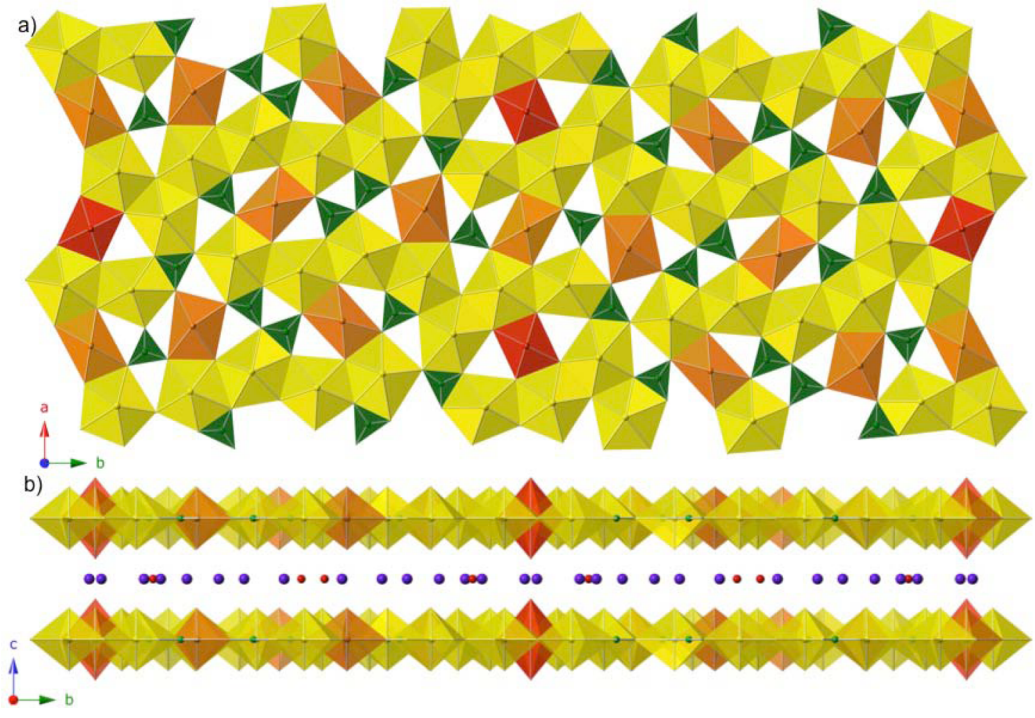

Figure 2. (a) View along the [*ab*] plane showing all of the coordination environments. (b) View of the interlayer containing K^+ cations and water molecules. U(VI) is represented by yellow and orange polyhedra, U(V) is represented by red polyhedra, borate is represented by green triangles, oxygen atoms are represented by red spheres, and K^+ cations are represented by blue spheres.

sharing between the fragments. Topologically, these additional groups are within the claw-like fragments (shown in orange), and this results in the bending of the U-chains. There is only a small difference between the UO_6 and UO_7 (mono and bidentate coordination on BO_3 triangle) positions within the claw-like fragments that causes the coordination change of uranium atoms. In the topological representation shown in Figure 2b, the space between A/B fragments is filled by triangular groups (shown in blue) and can be designated as the T-chain (triangular). Summing the chain groups, the topology

dx.doi.org/10.1021/ic500523a | *Inorg. Chem.* 2014, 53, 5294−5299

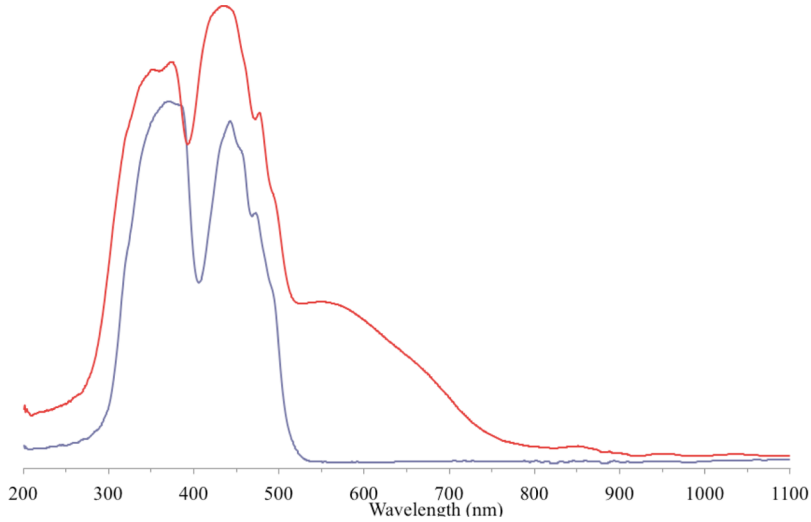

Figure 3. UV−vis−NIR absorption spectra for **1** (blue) and **2** (red). The broad feature centered at 550 nm is the charge-transfer band of U(V).

of $K_{10}[(UO_2)_{16}(B_2O_5)_2(BO_3)_6O_8]\cdot 7H_2O$ sheets can be described as ...PTPTPTP....

*$K_{13}[(UO_2)_{19}(UO_4)(B_2O_5)_2(BO_3)_6(OH)_2O_5]\cdot H_2O$ (**2**).* $K_{13}[(UO_2)_{19}(UO_4)(B_2O_5)_2(BO_3)_6(OH)_2O_5]\cdot H_2O$ (**2**) is a layered structure that crystallizes in the centrosymmetric, orthorhombic space group *Pbam*. The layers are composed of a complex sheet of uranium and boron that propagate parallel to the [*ab*] plane, with the inner layer occupied by potassium atoms and water molecules (Figure 2). The *b* axis is remarkably long at 49.867(3) Å because there are 11 crystallographically unique uranium sites. Seven of the uranium centers are surrounded by seven oxygen atoms, creating UO_7 pentagonal bipyramidal environments that are fairly regular in their geometries. The remaining four uranium atoms are found within UO_6 tetragonal bipyramids, and here the coordination can be highly distorted. The sheet topology is similar to that of $K[(UO_2)_{19}(UO_4)(B_2O_5)_2(BO_3)_6(BO_2OH)_{10}]\cdot nH_2O$.[19] However, **2** lacks the borate groups that bridge between the layers to create the three-dimensional network observed in $K[(UO_2)_{19}(UO_4)(B_2O_5)_2(BO_3)_6(BO_2OH)_{10}]\cdot nH_2O$. The replacement of the BO_3^{3-} linker with OH^- is accompanied by a lowering of the oxidation state of the uranium site to U(V). The U(V) center deviates from the typical uranyl geometry because it has four short equatorial bonds of 1.999(13) Å (×2) and 2.134(13) Å (×2) and two longer axial bonds of 2.33(3) Å, forming the tetraoxo core geometry (Figure 4a and 4b). The assignment of the pentavalent oxidation state to this uranium site is suggested by bond-valence sum calculations as well as spectroscopic data (vide infra). The bond-valence sum of the uranium within the $[UO_4(OH)_2]$ unit is 5.2, consistent with U(V). Additionally, in $K[(UO_2)_{19}(UO_4)(B_2O_5)_2(BO_3)_6(BO_2OH)_{10}]\cdot nH_2O$, the U8 site is present as a pentagonal bipyramid; however, in **2** the coordination is better described as 6 + 1, with four short bonds ranging from 2.25(1) Å to 2.38(2) Å and a long interaction of 2.74(2) Å. The other 10 uranium sites are found within classical uranyl cores, UO_2^{2+}, with two short axial bonds and much longer equatorial bonds. These uranyl distances range from 1.805(1) to 1.82(1) Å within the pentagonal bipyramids and from 1.78(1) to 1.81(2) Å within the tetragonal bipyramids. The equatorial interactions range from 2.23(1) to 2.73(2) Å and from 2.17(1) to 2.38(2) Å in the pentagonal and tetragonal bipyramids, respectively. The bond-valence sums for these 10 sites range from 5.79 to 6.18.

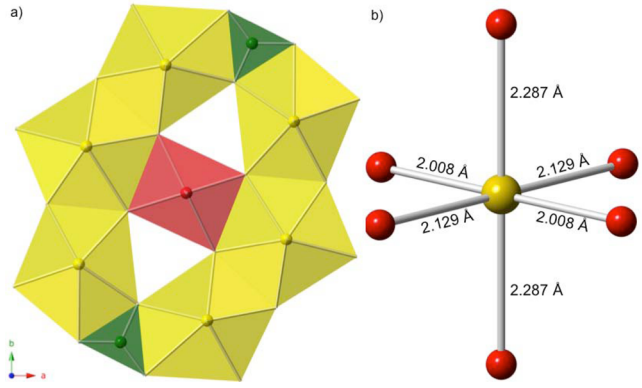

Figure 4. (a) View of the local coordination environment surrounding the tetraoxo core in $K_{13}[(UO_2)_{19}(UO_4)(B_2O_5)_2(BO_3)_6(OH)_2O_5]\cdot H_2O$ (**2**). (b) Ball and stick model of the tetraoxo core showing the four short and two long bonds.

A number of the uranium silicates and germanates prepared in supercritical water are mixed-valent and fall into two different classes. The first of these have ordered sites of different oxidation states and includes $Rb_3(U_2O_4)(Ge_2O_7)$.[20] In the second group, some of the uranium sites are formally intermediate-valent such as $Cs_2K(UO)_2Si_4O_{12}$.[21] A final group incorporates both ordered sites and intermediate sites such as $Cs_4(U^VO)(U^{IV/V}O)_2(Si_2O_7)_2$ and $Cs_x(U^VO)(U^{IV/V}O)_2(Ge_2O_7)_2$.[22] However, it is probably better to describe these as disordered because the most likely explanation is that each site represents an average of multiple oxidation states rather than true intermediate-valency. Compound **2** falls into the first category, and the mixed-valent sites are ordered. It is not entirely clear which group the neptunyl borates, $K_4(NpO_2)_{6.73}B_{20}O_{36}(OH)_2$ and $Ba_2(NpO_2)_{6.59}B_{20}O_{36}(OH)_2\cdot H_2O$,[23] fall into, but they are most likely disordered, placing them into the second category.

In contrast to uranyl borates prepared from boric acid flux reactions at much lower temperatures, BO_4 tetrahedral building units are absent in **2** and only BO_3 triangles are present. In addition, the borate does not form a polymeric network, and instead only BO_3 triangles and dimeric B_2O_5 units are found. The B−O bond distances range from 1.30(1) to 1.43(2) Å. It is well-known that high temperatures favor BO_3 units over BO_4,

dx.doi.org/10.1021/ic500523a | *Inorg. Chem.* 2014, 53, 5294−5299

and, in fact, of the uranyl borates prepared by Gasperin using reaction temperatures of ~1150 °C, only $Ni_7B_4UO_4$ possesses BO_4 tetrahedra.[24] All other compounds only contain BO_3 triangles. More recently, high-temperature and high-pressure studies of the Th−B−O and U−B−O systems have shown the presence of exclusively BO_4 at pressures above 5.5 GPa for Th and 10.5 for U.[25] The prevalence of BO_4 in these structures is a result of the extremely high pressures.

UV−Vis−NIR Absorbance Spectroscopy. The room-temperature UV−vis−NIR absorbance spectra shown in Figure 3 have two key regions. At short wavelengths, the classical absorption bands of uranyl exist. The first of these are the equatorial LMCT band centered near 350 nm. The second feature at 450 nm is the vibronically coupled transitions of the UO_2^{2+} core that have been extensively studied for more than 5 decades.[26,27] In the spectrum of **2**, but not **1**, there is a third broad peak centered at 550 nm that arises from the charge transfer of the U(V) unit. This transition has been observed in UCl_5 and is characteristic of U(V).[28] The typical *f*−*f* transitions of U(V) are not exhibited because the uranium resides on an inversion center, which strongly enforces the selection rules (*f*−*f* transitions are Laporte forbidden).

CONCLUSIONS

The formation of short oxo multiple bonds with metals occurs in order to stabilize high oxidation states. There are, in fact, variations in the number of oxo's required for a given oxidation state. For example, Mo(VI) most commonly has two oxo's to yield the *cis*-molybdenyl unit, MoO_2^{2+}, but molecules containing one oxo and three oxo's are known.[3] Uranyl is similar; two oxo's dominates U(VI) chemistry, yielding the trans, UO_2^{2+}, core, but U(VI) can be stabilized by a single oxo unit.[29] Oxidation states for metals beyond VI typically require four oxo atoms, as occurs for Np(VII) in $[NpO_4(OH)_2]^{3-}$.[30] The nearly planar nature of this tetraoxo core is unique to the actinide series. Therefore, the question becomes why is U(V) found within a tetraoxo core like Np(VII)? At most it should only require two oxo's for stabilization; one is probably sufficient. The answer is rather straightforward: These units are not isolated within molecules, but rather they are found within extended structures. The four short equatorial bonds are not to terminal oxo's, as found in $[NpO_4(OH)_2]^{3-}$, but rather the oxo's bound to U(V) actually bridge between three uranium centers (i.e., they are μ_3-oxo's). Thus, they are, in fact, helping to stabilize one U(V) and two U(VI) centers.

Although it is true that both mild and supercritical hydrothermal conditions provide access to U(V) compounds, it appears that there is a stability window for this oxidation state. $K[(UO_2)_{19}(UO_4)(B_2O_5)_2(BO_3)_6(BO_2OH)_{10}]\cdot nH_2O$, for example, was prepared using a reaction temperature that was only 50 °C higher than that used to prepare **2**.[19] This former compound is similar to **2**, but it lacks the U(V) center and contains only U(VI). In addition to the stability window issue, the syntheses of these compounds are all the more difficult because the reductant is generated in situ. The first example of a U(V) compound in this class was intentionally generated by using zinc metal as a reductant.[22] In contrast, in the supercritical reactions, the reducing agent is currently being debated and hence control is lacking.[15−17] Lastly, the high pH of these reactions is certainly playing a role in the stability window of U(V). Future studies should focus in part on better control of the reductive processes.

ASSOCIATED CONTENT

Supporting Information

Views through the top and side of **2**; linking of edge-sharing uranium chains via corner sharing and borate triangles to form a complex sheet topology; SEM images and EDS spectra of **1** and **2**; Raman spectra of **1** and **2**; selected bond valance sums for **1** and **2**; selected bond lengths and angles for **1** and **2**; thermal displacement values for **1** and **2**; atomic coordinates for **1**; and X-ray crystallographic data in CIF format. This material is available free of charge via the Internet at http://pubs.acs.org.

AUTHOR INFORMATION

Corresponding Authors

*E-mail: e.alekseev@fz-juelich.de (E.V.A.).
*E-mail: albrecht-schmitt@chem.fsu.edu (T.E.A.-S.).

Notes

The authors declare no competing financial interest.

ACKNOWLEDGMENTS

We are grateful for the support provided by the Chemical Sciences, Geosciences, and Biosciences Division, Office of Basic Energy Sciences, Office of Science, Heavy Elements Chemistry Program, U.S. Department of Energy under grant DE-FG02-13ER16414. E.V.A. is grateful to the Helmholtz Association for the support within the VH-NG-815 grant.

REFERENCES

(1) *The Chemistry of the Actinide and Transactinide Elements*; Morss, L. R., Edelstein, N. M., Fuger, J., Eds.; Springer: Dordrecht, The Netherlands, 2006.
(2) MacDonald, M. R.; Fieser, M. E.; Bates, J. E.; Ziller, J. W.; Furche, F.; Evans, W. J. *J. Am. Chem. Soc.* **2013**, *135*, 13310−13313.
(3) Cotton, F. A.; Wilkinson, G. *Advanced Inorganic Chemistry*, 5th ed; John Wiley & Sons: New York, 1988.
(4) Ilton, E. S.; Haiduc, A.; Cahill, C. L.; Felmy, A. R. *Inorg. Chem.* **2005**, *44*, 2986−2988.
(5) Chen, C. S.; Lee, S. F.; Lii, K. H. *J. Am. Chem. Soc.* **2005**, *127*, 12208−12209.
(6) (a) Belai, N.; Frisch, M.; Ilton, E. S.; Ravel, B.; Cahill, C. L. *Inorg. Chem.* **2008**, *47*, 10135−10140. (b) Camp, C.; Antunes, M. A.; Garcia, G.; Ciofini, I.; Santos, I. C.; Pecaut, J.; Almeida, M.; Marcalo, J.; Mazzanti, M. *Chem. Sci.* **2014**, *5*, 841−846. (c) Lukens, W. W.; Edelstein, N. M.; Magnani, N.; Hayton, T. W.; Fortier, S.; Seaman, L. A. *J. Am. Chem. Soc.* **2013**, *135*, 10742−10754. (d) Jilek, R. E.; Spencer, L. P.; Lewis, R. A.; Scott, B. L.; Hayton, T. W.; Boncella, J. M. *J. Am. Chem. Soc.* **2012**, *134*, 9876−9878. (e) Fortier, S.; Brown, J. L.; Kaltsoyannis, N.; Wu, G.; Hayton, T. W. *Inorg. Chem.* **2012**, *51*, 1625−1633. (f) Mougel, V.; Pecaut, J.; Mazzanti, M. *Chem. Commun.* **2012**, *48*, 868−870. (g) Fortier, S.; Kaltsoyannis, N.; Wu, G.; Hayton, T. W. *J. Am. Chem. Soc.* **2011**, *133*, 14224−14227. (h) Nocton, G.; Horeglad, P.; Vetere, V.; Pecaut, J.; Dubois, L.; Maldivi, P.; Edelstein, N. M.; Mazzanti, M. *J. Am. Chem. Soc.* **2010**, *132*, 9876−9878.
(7) Lee, C. S.; Lin, C. H.; Wang, S. L.; Lii, K. H. *Angew. Chem., Int. Ed.* **2010**, *49*, 4254−4256.
(8) Burns, P. C. *Can. Mineral.* **2005**, *43*, 1839−1894.
(9) Burns, P. C.; Ewing, R. C.; Hawthorne, F. C. *Can. Mineral.* **1997**, *35*, 1551−1570.
(10) Polinski, M. J.; Grant, D. J.; Wang, S.; Alekseev, E. V.; Cross, J. N.; Villa, E. M.; Depmeier, W.; Gagliardi, L.; Albrecht-Schmitt, T. E. *J. Am. Chem. Soc.* **2012**, *134*, 10682−10692.
(11) Wang, S.; Alekseev, E. V.; Depmeier, W.; Albrecht-Schmitt, T. E. *Chem. Commun.* **2011**, *47*, 10874−10885.
(12) Wang, S.; Alekseev, E. V.; Ling, J.; Skanthakumar, S.; Soderholm, L.; Depmeier, W.; Albrecht-Schmitt, T. E. *Angew. Chem., Int. Ed.* **2010**, *49*, 1263.

(13) Kolis, J. W.; Korzenski, M. B.; Synthesis of inorganic solids. In *Chemical Synthesis Using Supercritical Fluids*; Jessop, P. G.; Leitner, W., Eds.; Wiley-VCH Verlag GmbH: Weinheim, Germany, 2007; pp 213−242.
(14) Franck, E. U. *Fluid Phase Equilib.* **1983**, *10*, 211−222.
(15) *Hydrothermal Synthesis of Crystals*; Lobachev, A. N., Ed.; Consultants Bureau: New York, 1971; p 80.
(16) Rabenau, A. *Angew. Chem., Int. Ed. Engl.* **1985**, *24*, 1026−1040.
(17) Rabenau, A. *J. Mater. Educ.* **1988**, *10*, 543−591.
(18) Leonyuk, N. I. *J. Cryst. Growth* **1997**, *174*, 301−307.
(19) Burns, P. C. *Rev. Mineral.* **1999**, *38*, 23−90.
(20) Wu, S.; Wang, S.; Polinski, M.; Beermann, O.; Kegler, P.; Malcherek, T.; Holzhied, A.; Depmeier, W.; Bosbach, D.; Albrecht-Schmitt, T. E.; Alekseev, E. V. *Inorg. Chem.* **2013**, *52*, 5110−5118.
(21) Lin, C. H.; Lii, K. H. *Angew. Chem., Int. Ed.* **2008**, *120*, 8839−8841.
(22) Lee, C. S.; Wang, S. L.; Lii, K. H. *J. Am. Chem. Soc.* **2009**, *131*, 15116−15117.
(23) Chen, C. L.; Nguyen, Q. B.; Chen, C. S.; Lii, K. H. *Inorg. Chem.* **2012**, *51*, 7463−7465.
(24) Gasperin, M. *Acta Crystallogr.* **1989**, *C45*, 981−983.
(25) Hinteregger, E.; Hofer, T. S.; Heymann, G.; Perfler, L.; Kraus, F.; Huppertz, H. *Chem.—Eur. J.* **2012**, *19*, 15985−25992.
(26) Liu, G.; Beitz, J. V. Spectra and electronic structures of free actinide atoms. In *The Chemistry of the Actinide and Transactinide Elements*; Morss, L. R., Edelstein, N. M., Fujer, J., Eds.; Springer: Dordrecht, The Netherlands, 2006; Vol. *4*, Chapter 16, pp 2013−2111.
(27) Carnall, W. T.; Liu, G. K.; Williams, C. W.; Reid, M. F. *J. Chem. Phys.* **1991**, *95*, 7194−7203.
(28) Leung, A. F.; Poon, Y. M. *Can. J. Phys.* **1977**, *55*, 937−942.
(29) (a) de Wet, J. F.; du Preez, J. G. H. *J. Chem. Soc., Dalton Trans.* **1978**, 592. (b) Arney, D. S. J.; Burns, C. J. *J. Am. Chem. Soc.* **1995**, *117*, 9448. (c) Fortier, S.; Kaltsoyannis, N.; Wu, G.; Hayton, T. W. *J. Am. Chem. Soc.* **2011**, *133*, 14224−14227.
(30) Williams, C. W.; Blaudeau, J.-P.; Sullivan, J. C.; Antonia, M. R.; Bursten, B.; Soderholm, L. *J. Am. Chem. Soc.* **2001**, *123*, 4346−4347.